INSTITUTE OF PHYSICS PUBLISHING JOURNAL OF PHYSICS D: APPLIED PHYSICS

J. Phys. D: Appl. Phys. **38** (2005) 2597–2605 doi:10.1088/0022-3727/38/15/010

The effect of multiple scattering on velocity profiles measured using Doppler OCT

J Moger[1], S J Matcher[1], C P Winlove[1] and Angela Shore[2]

[1] Biomedical Physics Group, University of Exeter, Exeter, EX4 4QL, UK
[2] Peninsular Medical School, Institute of Biomedical and Clinical Science, Exeter, EX2 5AX, UK

E-mail: J.Moger@Exeter.ac.uk

Received 26 November 2004, in final form 1 March 2005
Published 22 July 2005
Online at stacks.iop.org/JPhysD/38/2597

Abstract

In this paper we investigate the effect of multiple scattering on Doppler optical coherence tomography (DOCT) images of model blood vessels embedded in a medium with optical properties similar to those of the human dermis. Furthermore, we quantify the deviation of the acquired velocity profiles from that known to exist within a glass capillary at various depths within the scattering media.

A flow phantom consisting of a glass tube containing whole blood flowing under laminar conditions submerged in a variable depth of Intralipid was used to simulate a blood vessel within the cutaneous microcirculation. DOCT images and velocity profiles of the tube acquired at various depths within the Intralipid are compared with those obtained from the same tube in a non-scattering medium with the same refractive index.

1. Introduction

Doppler optical coherence tomography (DOCT) is a technique for simultaneously performing real-time high-resolution imaging of tissue structure and blood flow [1–3]. Using this technique, fluid velocity profiles [4–7] and shear-rates [8] have been recorded in flow phantoms and *in vivo* systems [9,10]. We have previously shown that DOCT can detect subtle changes in the velocity profile of red blood cell suspensions as functions of the mean flow velocity, cell concentration and cell rigidity in phantoms with diameters as small as several hundred micrometres [11]. Accurate *in vivo* measurement of blood velocity profiles within the microcirculation is required to estimate volume flow rate and effective haematocrit through small vessels [12]. Before the development of DOCT, *in vivo* measurements of velocity in the cutaneous circulation relied predominantly upon microscopy techniques [13, 14]. These techniques require time consuming post-acquisition analysis of the distances moved by individual particles between video frames and so do not allow real-time monitoring of flow dynamics on a biological time scale or in larger vessels which cannot be visualized.

Due to the non-invasive nature of DOCT, it has great potential for investigating the delicate blood flow dynamics thought to exist within the cutaneous microcirculation, an area previously inaccessible due to the high level of optical scattering. Although DOCT has a high scattered light rejection ratio, it is possible that in highly scattering tissues photons may undergo more than one scattering event, causing the apparent backscattered position ascribed to the detected photon to differ from any one of the true scattering events. Furthermore, the total Doppler shift reported by a multiple scattered photon will differ from that reported by photons undergoing single backscattering events if the second scattering event is also from a moving particle.

Using a tissue phantom we investigate the applicability of DOCT to the human dermis by examining the effect of multiple scattering upon cross-sectional DOCT images of a tube containing whole blood flowing under laminar conditions. By considering the fitting statistics of a parabolic velocity profile, we quantify the accuracy to which velocity profiles can be fitted as a function of depth into the phantom. Furthermore, we ascertain whether the complex flow dynamics of red blood cells thought to exist in small blood vessels could be measured *in vivo*.

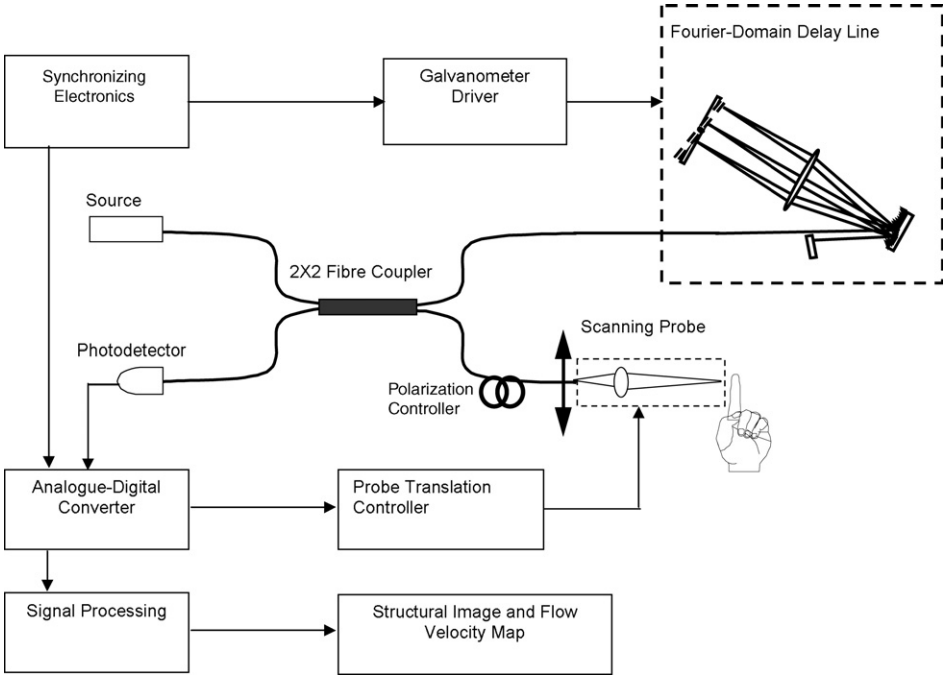

Figure 1. Schematic of the Doppler OCT system and signal processing apparatus.

2. Materials and methods

A schematic of the DOCT system used in this investigation is provided in figure 1. The Michelson interferometer consists of a 2 × 2 fibre coupler that provides a stable interferogram with minimal interference from vibration and thermal air currents. The source was an amplified spontaneous emission (ASE0 laser (B&W Tek Inc.)) with an optical output power of 7 mW and a spectral full width half maximum of 100 nm centred at 1550 nm, producing a coherence length of approximately 15 μm in air. Reference arm scanning was achieved by a Fourier-domain delay-line [15], which uses a diffraction grating and a galvanometer to generate an optical path difference of 1–2 mm with a maximum axial scan rate of 500 Hz. The sample arm probe consisted of an objective lens with a numerical aperture of 0.12, yielding a lateral resolution of approximately 20 μm. The lateral motion used to produce images from sequential line-scans was achieved by mounting the lens upon a voice coil translation stage (Physik Instruments).

Line-scans corresponding to a physical depth of 1 mm were acquired with a repetition rate of 5 Hz. Line-scans, consisting of 6400 data points, were sampled at 32 kHz and divided into 100 pixels, each 64 data points in length. A spectrogram of each pixel was produced using a short-time Fourier transform (STFT) algorithm, yielding a frequency bin separation corresponding to a velocity of approximately 1 mm s^{-1}. The optical coherence tomography (OCT) and DOCT images were processed using the spectrogram method. For the OCT images, the value in each pixel was obtained by taking the base 10 logarithm of the amplitude of the power spectrum at the reference frequency. The OCT image was then displayed using a 64 colour-level grey-scale colour-map with the maximum and minimum colour values determined by the maximum and minimum values of the image pixels. The intensities for the DOCT image pixels were calculated from the shift in the position of the centre of gravity of the spectrum from the reference frequency, and the frequency shifts were then converted into velocities. The DOCT images were displayed using a 64 level false-colour-map.

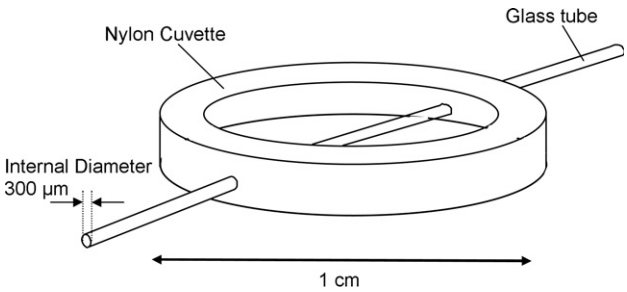

Figure 2. Simplified simulation of a blood vessel in the human dermis, consisting of a glass capillary immersed in a solution of Intralipid-20%.

The phantom, shown in figure 2, provided a simplified simulation of a large blood vessel located in the human dermis. A glass capillary with an internal diameter of 300 μm was set into a shallow cuvette containing Intralipid solution at 20% by volume. At this concentration Intralipid [16] has a scattering coefficient of 11.2 mm^{-1}, approximating the average scattering properties of the human dermis [17, 18]. The depth of the capillary below the surface of the Intralipid was altered by varying the volume of the solution in the cuvette. Heparinated whole human blood taken from healthy volunteers was passed through the capillary at room temperature (∼20°C), using an infusion pump which provided flow at a known constant velocity. The infusion pump was set so that the blood passed through the capillary with a mean flow velocity of 7.5 mm s^{-1}. Fluid mechanics predicts that at this flow rate the blood cells will have a parabolic velocity profile [19].

To allow direct comparison of measurements with and without external scattering, the non-scattering data were obtained with the capillary immersed in distilled water to approximate the refractive index of the Intralipid. A refractive index of 1.4 was used to convert optical path differences within the Intralipid, distilled water and blood into physical distances used to measure the depth of the scattering media.

The sample arm beam was focused on the centre of the capillary at an angle of 45° to the direction of flow. Velocity profiles were obtained by averaging 100 DOCT line-scans through the centre of the capillary.

Cross-sectional OCT and DOCT images centred on the capillary were acquired by laterally translating the probe by 500 μm from the centre of the capillary and acquiring 100 line-scans each separated by lateral steps of 10 μm in the opposite direction. The line-scans were processed to produce a grey scale structural OCT image and a colour DOCT velocity map of the tube.

The distilled water was replaced by Intralipid 20%, with the glass capillary just beneath the surface. Velocity profiles and images were recorded with the same parameters used for the non-scattering phantom. Intralipid was added in three further increments until measurements were obtained with the capillary 800 μm beneath the surface of the Intralipid.

As the depth of the Intralipid was increased the sample arm focus was moved by a distance equivalent to the refractive index adjusted optical path difference of the Intralipid solution. The reference arm mirror was then moved to compensate for the resulting change in optical path length. In addition to compensating for path length, the reference arm was adjusted to balance the dispersion in the sample and reference arms as the depth of Intralipid was increased [15].

3. Data processing and analysis

3.1. Images

The degradation in image quality caused by multiple scattering in the Intralipid was evaluated qualitatively by visual comparison between the images obtained in the presence and absence of the scattering media .

3.2. Velocity profiles

The velocity profiles were obtained by averaging the reference peak Doppler shift in each pixel over the 100 line-scans. The average frequency shifts were then converted into velocities using equation (1):

$$v = \frac{f_s \lambda_0}{2 n_s \cos\theta}, \tag{1}$$

where λ_0 is the central wavelength of the source, n_s is the local refractive index of the sample, f_s is the average frequency shift and θ is the angle between the sample arm beam and the direction of flow.

Fluid mechanics predicts that whole blood flowing with an average velocity of 7.5 mm s^{-1} in a tube of this diameter exhibits a parabolic velocity profile [19]. In order to quantify the effect of Doppler noise caused by multiple scattering, the velocity profiles from each depth of Intralipid were compared with the parabolic velocity profile expected for whole blood flowing under these conditions. The extent to which the distorted profiles deviated from the predicted parabolic profile was quantified by the chi-squared value.

The 'true' flow profile, undistorted by multiple scattering outside the capillary, was obtained by fitting a parabola to the Doppler shifts obtained from inside the tube immersed in water. This was achieved using software based on the Levenberg–Marquardt algorithm to fit equation (2) to the recorded data; the fit was weighted using the standard deviation of each point calculated from the 100 line-scans over which the velocity prfile was averaged.

$$V(r) = V_{\max}\left(1 - \left|\left(\frac{r}{R}\right)\right|^2\right), \qquad -1 \leqslant \frac{r}{R} \leqslant 1, \tag{2}$$

where $V(r)$ is the velocity at radial position r, $V_{\max}$ is the velocity at the centre of the tube and R is the radius of the tube. This stage of analysis was also used to verify that the blood cells did indeed exhibit a parabolic velocity profile and to measure exact values of the peak flow rate and the internal diameter of the glass capillary. Any observed error in the fitted data at this stage will be due to Doppler shifts caused by multiple scattering within the blood and the finite signal-to-noise ratio of our system.

If multiple scattering of photons within the Intralipid does indeed cause the measured velocity profiles to become distorted, it would be useful to quantify the accuracy to which parametrization of these profiles could be achieved. This will determine whether subtle changes in the velocity profile could be measured *in vivo*. Again using the Levenberg–Marquardt algorithm, equation (3), modified from [13], was fitted to each profile.

$$V(r) = V_{\max}\left(1 - \left|a\left(\frac{r}{R}\right)\right|^K\right), \qquad -1 \leqslant \frac{r}{R} \leqslant 1, \quad a \geqslant 0, \tag{3}$$

where $V(r)$ is the velocity at radial position r, $V_{\max}$ is the velocity at the centre of the tube and R is the radius of the tube. The scaling factor a is used to allow non-zero intercept fit with the tube wall. The shape of the profile is described by the parameter K: a parabolic velocity distribution corresponds to $K = 2$, and K increases as the profile becomes progressively flatter. Values for the capillary radius and peak flow velocity were taken from the undistorted profiles. Again, each fit was weighted with the standard deviation at individual points across the capillary.

The fitted value of the parameter K shows the degree to which multiple scattering has caused the fitting algorithm to misinterpret the 'true' shape of the velocity profile. A value of 2 corresponds to correct interpretation of the parabolic profile, and any significant deviation from 2 shows that the profile has been misinterpreted. This parameter has previously been used to describe the deviation of red blood cells from parabolic flow due to changes in the cell velocity [13] and rigidity [11]. Therefore the knowledge of any significant systematic deviation of the parameter K from a value of 2 caused by multiple scattering is important to the vascular clinician. Equation (2), modelling the 'true' parabolic profile known to exist within the capillary, is initially fitted to each profile and the chi-squared values used to show if increasing the capillary depth indeed causes a reduction in signal quality.

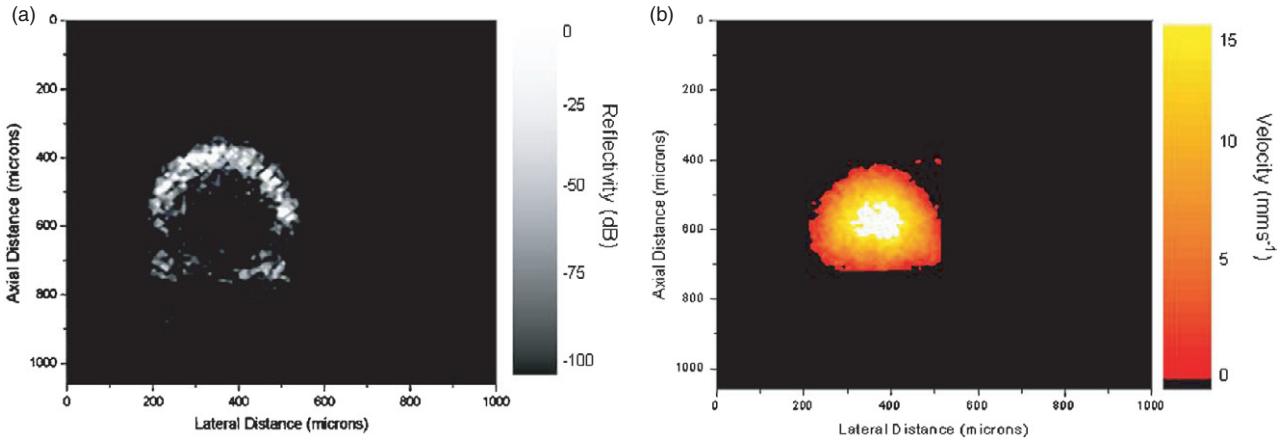

Figure 3. (*a*) and (*b*) show OCT and DOCT images, respectively, of the capillary containing whole blood flowing with an average velocity of 7.5 mm s^{-1} immersed in a non-scattering medium with a refractive index similar to that of the tissue phantom.
(This figure is in colour only in the electronic version)

The same profiles are then fitted with equation (3), where the model is no longer constrained to a parabola, and any deviation of the fitted value of the parameter K from 2 shows the extent to which multiple scattering causes misinterpretation of the shape of the profile.

The standard error measured over the 100 line-scans used to calculate the average velocity at each pixel was used to weight the value of chi-squared and to calculate the error in the fitted values of K. The significance of the chi-squared values for each fit were calculated using confidence level tables for the chi-squared distribution. Weighting chi-squared with the standard deviation at each point should take into account the increased signal-to-noise ratio with capillary depth. This will confirm whether the distortion in the velocity profiles is indeed a systematic effect of multiple scattering or caused by an overall reduction in fitting accuracy due to signal attenuation in the Intralipid.

The following analysis was performed in order to verify that weighting the chi-squared values for each fitted profile could indeed be used to take into account the decrease in signal-to-noise with increased Intralipid depth. To simulate the effect of a reduced signal-to-noise ratio independent of the effects of multiple scattering, a velocity profile of the capillary immersed in water averaged over 100 line-scans was compared with the same velocity profile averaged over 10 line-scans. Reducing the number of line-scans over which the profile was averaged by a factor of 10 simulates a 10-fold reduction in the signal-to-noise ratio and should increase the standard deviation at each point by an approximate factor of 3. If the chi-squared values are weighted with the corresponding standard errors, both velocity profiles should have similar chi-squared values despite the apparent inferior fitting quality of the profile averaged over fewer line-scans.

4. Results

In vitro images and velocity profiles of the blood flow in the glass capillary at four depths within the tissue phantom are compared with those obtained for the same capillary in the non-scattering medium. The depths of the capillary beneath the surface of the phantom, obtained from the OCT images, were 50, 150, 300 and 800 μm. The capillary depth within the non-scattering medium was sufficient for the air–water interface not to appear in the images.

4.1. OCT and DOCT images

Figure 3 shows the OCT and corresponding DOCT images of whole blood flowing with a mean velocity of 7.5 mm s^{-1} through the capillary immersed in distilled water. Figure 4 shows OCT and DOCT images of the blood flow within the capillary at depths of 50, 150, 300 and 800 μm below the surface of the tissue phantom.

4.2. Velocity profiles

Figure 5 compares the velocity profiles of the capillary immersed in water averaged over (*a*) 100 and (*b*) 10 line-scans. Figure 6 shows velocity profiles fitted with equation (2) to show how the fitting quality of the correct model decreases as a function of capillary depth in the scattering media. Profile (*a*) was measured with the capillary immersed in water, and profiles (*b*), (*c*), (*d*) and (*e*) with the capillary at depths of 50, 150, 300 and 800 μm within the Intralipid.

The same velocity profiles presented in figure 6 fitted with the model described by equation (3) are shown in figure 7. The error bars represent the standard error at each point calculated from the 100 line-scans used to generate the data. The solid line illustrates the fitted velocity profiles. The undistorted profile (*a*) is fitted with a parabola; as the capillary depth increases from 50 μm (*b*) to 800 μm (*e*), the best fit model becomes increasingly 'blunted'. This suggests that multiple scattering effects may introduce systematic errors in the measured velocity profiles. A significant difference between the 'true' and measured K appears beyond a depth of 150 μm, or 2.55 scattering mean-free-paths.

5. Discussion

The OCT image of the capillary immersed in water contains a slightly blurred annular structure which corresponds to the

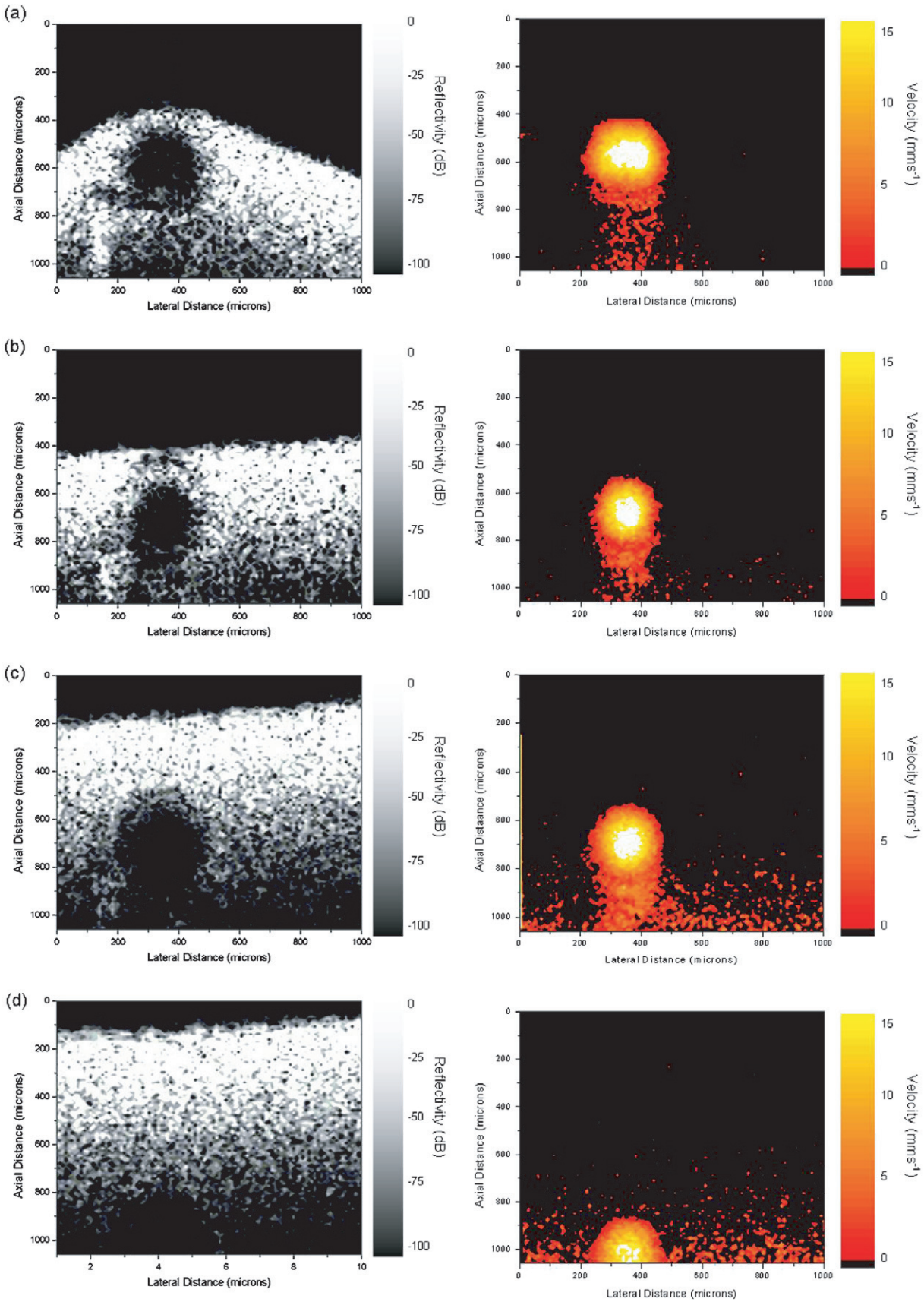

Figure 4. (*a*), (*b*), (*c*) and (*d*) show (left) OCT and (right) DOCT images of the glass capillary immersed 50, 150, 300 and 800 μm below the surface of the scattering tissue phantom.
(This figure is in colour only in the electronic version)

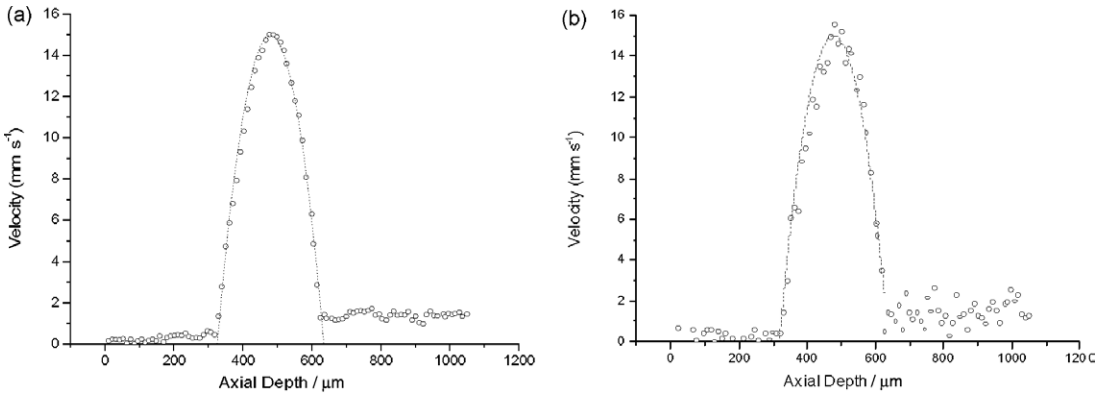

Figure 5. Velocity profiles of the capillary immersed in water averaged over (*a*) 100 line-scans and (*b*) 10 line-scans fitted with a parabolic flow model, i.e. equation (2), with respective chi-squared values of 13.6 and 16.7.

glass walls. The centre of the capillary appears empty due to the signal from the moving red blood cells having been Doppler shifted away from the reference frequency. If the system were to have infinite spatial resolution, one would expect the image to consist of two infinitely thin concentric rings corresponding to the internal and external walls of the capillary. However, although the axial resolution of the system, calculated to be around 10 μm, is less than the thickness of the glass wall, which is estimated to be of the order of several tens of micrometres, the inner and outer walls appear as one blurred interface. This 'blurring' can be explained by the presence of side-lobes in the axial point spread function (PSF), arising from a non-Gaussian spectrum of the source that cause a small, but not insignificant, reduction in the system's axial resolution. Further blurring could arise from a slight residual mismatch in dispersion between the sample and reference arms that was not completely compensated when the depth of imbedding media was changed. Stationary red blood cells at the capillary wall obeying the non-slip condition also contribute to the image blurring, as well as those moving close to the wall with a sufficiently low velocity that does not exceed the velocity resolution and hence appear to be stationary. The combined effect of the capillary wall thickness approaching the system's axial resolution and the presence of stationary red blood cells causes the appearance of scattering in the glass walls of the capillary. This 'false' signal could be avoided by reducing the PSF (i.e. using a source with a longer coherence length or a Gaussian power spectrum) or by increasing the capillary wall thickness.

The DOCT image of the capillary in water contains concentric annular regions of equal velocity which increase from zero at the capillary wall to a maximum at the centre of the capillary corresponding to twice the average flow velocity. The capillary walls do not appear in this image due to their un-shifted signal appearing in the static background, represented in this case by the black region of the colour map. Again there is some blurring at the capillary walls due to the low flow velocity and finite velocity sensitivity of the system. The finite velocity resolution also causes blurring of the annular regions of equal flow velocity.

The OCT images of the glass capillary immersed in the various depths of Intralipid solution all clearly show the region of the capillary containing flowing Intralipid as an area of zero intensity due to the signal from moving scatterers being Doppler shifted from the reference frequency. Blurring at the internal glass/blood interface again occurs due to the non-slip condition. As the capillary depth is increased there is an increasing amount of false stationary signal, or 'noise', appearing within the internal wall of the capillary. This is due to multiple scattering of photons above the capillary, causing their measured path length to be greater than the depth of any one of the scattering sites and hence appear in the region of the image where a stationary signal would otherwise not be expected. A shadow appears in the region of Intralipid directly beneath the capillary; this again may be due to multiple scattering of photons. Photons that experience multiple scattering between the surface of the Intralipid and the bottom of the capillary not only appear at a greater depth than expected, but may have also experienced Doppler shifts from the blood within the capillary, hence causing their signal to become shifted beyond the reference frequency. The effects of a reduction signal-to-noise ratio beneath the capillary may also contribute to this shadowing effect. The effect of a reduction in signal-to-noise ratio as a function of depth is not quantified for the DOCT images in this investigation. However, standard error weighting is used to eliminate these effects during the analysis of the velocity profiles.

The regions of the DOCT images containing the flow are clearly visible at all four depths within the scattering medium. The characteristic annular pattern of the parabolic flow becomes increasingly distorted at greater depths, which may be due to the occurrence of multiple scattering events that cause both falsely registered depths and Doppler shifts. The region directly beneath the capillary, appearing as a shadow in the OCT images, contains Doppler shifted pixels which give the impression that there may be fluid flow under the capillary. The density and Doppler shift of these pixels increase with depth. Again, this artefact may be due to the occurrence of multiple scattered photons causing false registration of both depth and Doppler shift. Again, both these artefacts may be due to a reduced signal-to-noise ratio beneath the capillary and scattering within the capillary.

In all the DOCT images, both in the scattering and non-scattering phantoms, the lower 200 μm contains falsely registered Doppler shifted pixels. This is because the backscattered signal intensity, attenuated by the sample, approaches the system's noise floor, hence causing the centroid

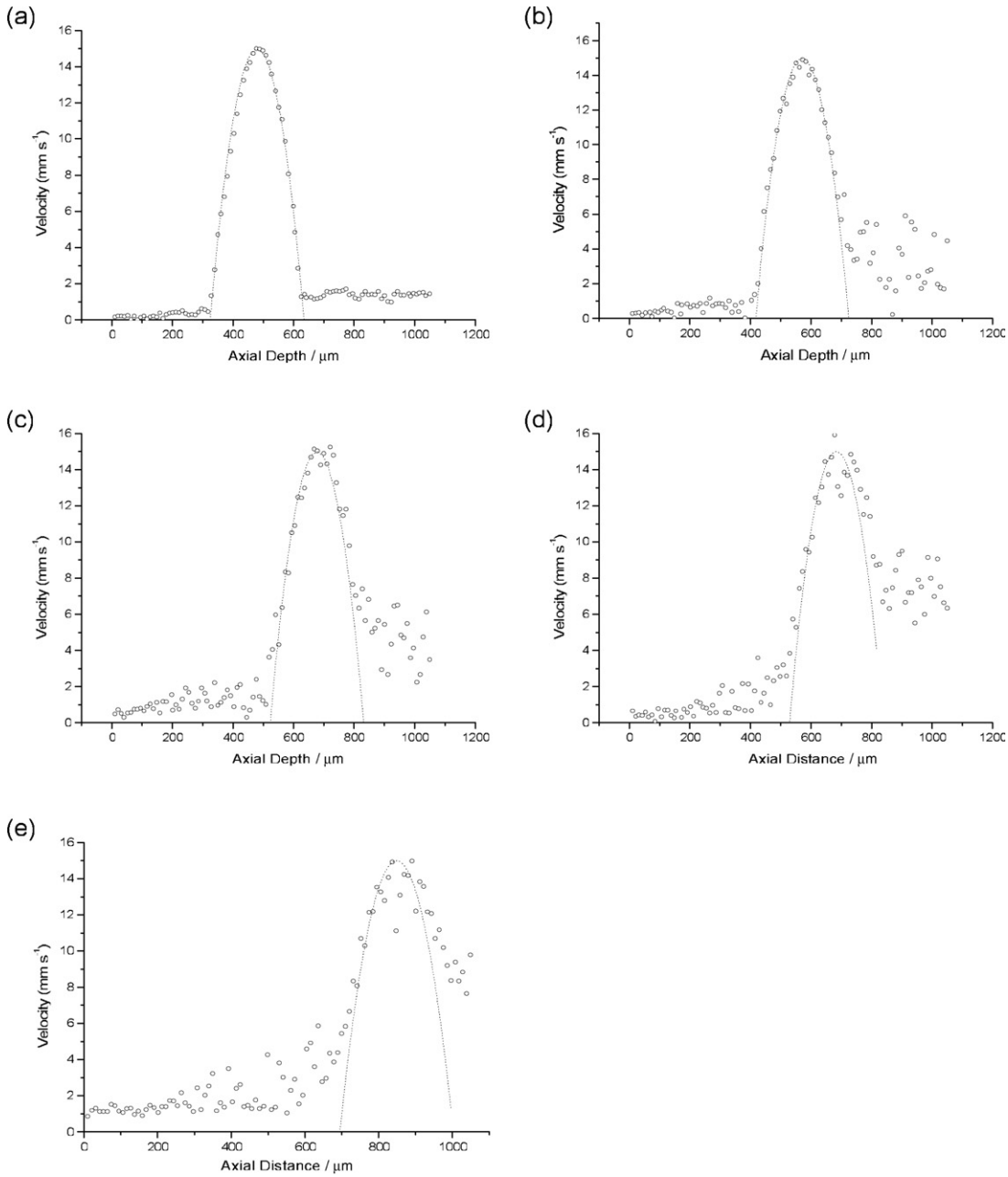

Figure 6. (*a*) Fitted velocity profile of the capillary immersed in the non-scattering phantom: chi-squared value 13.6. (*b*)–(*e*) Fitted velocity profiles obtained from depths 50 μm, 150 μm, 300 μm and 800 μm below the surface of the scattering phantoms: respective chi-squared values 22.5, 31.1, 34.1 and 40.7.

detection algorithm to falsely locate the peak frequency. The attenuation is visible in the corresponding OCT images, where the same region appears to fade away and become dominated by system noise.

Figure 5(*a*) shows the velocity profile obtained from the capillary in the non-scattering phantom averaged over 100 line-scans. This profile shows excellent agreement with the predicted parabolic model, with a chi-squared of approximately 14, which corresponds to a confidence limit of 99.7%. Although having the appearance of dramatically reducing the goodness of fit, simulating a 10-fold reduction in signal-to-noise ratio independent of multiple scattering does not significantly reduce the confidence limit of the fitted model. Figure 5 (*b*) has a weighted chi-squared value of approximately 17, which corresponds to a confidence limit of 97.5%. This shows that a lower signal-to-noise, and hence a higher standard error, has little effect on the confidence limit of the fitted model, if chi-squared is property weighted. Therefore, it is reasonable to assume that a reduction in weighted chi-squares as the capillary depth is increased can be attributed to multiple scattering.

As the depth of the capillary within the Intralipid increases, the goodness of the fit deteriorates to a maximum chi-squared value of 41 at a depth of 800 μm, this corresponds to a confidence limit of only 15.6%. The confidence limits associated with the chi-squared values show that at depths

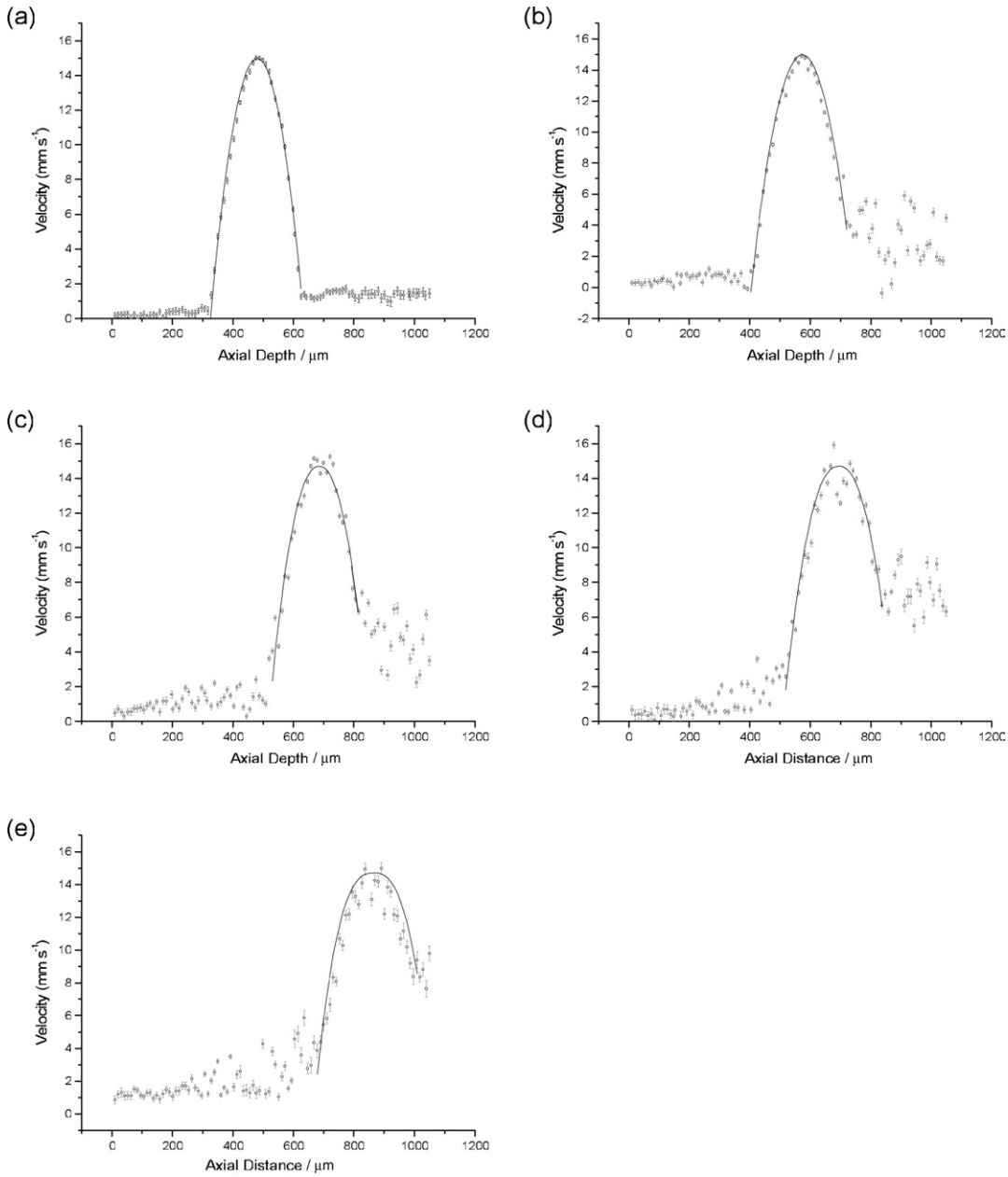

Figure 7. Velocity profiles from figure 6 parametrized using equation (3). Error bars show the standard deviation at each point calculated from the 100 line-scans from which each data point was averaged. The fitting results are as follows: (*a*) $K = 2.01 \pm 0.05$, chi-squared = 13.6, (*b*) $K = 2.09 \pm 0.07$, chi-squared = 21.2, (*c*) $K = 2.2 \pm 0.12$, chi-squared = 30.3, (*d*) $K = 2.3 \pm 0.17$, chi-squared = 32.3, (*e*) $K = 2.7 \pm 0.21$, chi-squared = 39.8.

greater than 150 μm the probability of the profile being parabolic is less than 56%.

The deviation from the expected parabolic profile can be explained by the same multiple scattering processes that were used to describe the presence of noise in the DOCT images. The falsely registered Doppler shifts occurring below the capillary are also present in the velocity profile plots and increase with capillary depth.

The value of the fitting parameter K for the capillary immersed in water is equal to 2.01. The error on this value, ± 0.05, is due to noise in the measured velocity caused by attenuation in the blood and the finite velocity resolution of the system. As predicted, the value of K in the non-scattering medium corresponds to a parabola. This confirms that the capillary does indeed support laminar flow at a flow velocity of 7.5 mm s^{-1}. Immersing the capillary in 50 μm of Intralipid-20% has very little effect upon the fitted value of K, which does not change significantly beyond the fitting error of ± 0.07. It is not surprising that this small depth of Intralipid has little effect, as it is small in comparison with the scattering mean free path of the Intralipid. Increasing the capillary depth to 150 μm causes the fitting algorithm to interpret the parameter K as 2.2, a deviation greater than the error margin of ± 0.10 from the expected value of 2. At depths of 300 μm and 800 μm the misinterpretation increases, producing K values of 2.3 and 2.7, respectively. In the two cases the deviation from 2 exceeds

the fitting errors of ± 0.17 and ± 0.21, respectively. The value of chi-squared increases with the depth of the capillary beneath the surface of the Intralipid. Although the chi-squared values of the non-parabolic model at depths greater than 150 μm show extremely low probabilities, they are higher than those for the same data fitted with the parabolic model. While the non-parabolic models appear to be a closer fit than the parabolic models, neither have sufficient confidence limits to be considered an accurate model. This merely shows that at depths greater than 150 μm the error on the Doppler shift caused by multiple scattering causes the fitting procedure to become unreliable.

Interestingly, in all three cases where multiple scattered photons cause the shape of the velocity profile to become misinterpreted, the fitting parameter K is greater than the expected value. These results suggest that if velocity profiles were to be measured in a scattering medium at depths greater than 150 μm, i.e. the upper dermal plexus, multiple scattering of photons would have the effect of increasing the degree of blunting observed in the measure velocity profiles.

The estimation of 150 μm as the maximum depth at which subtle changes in flow profiles can be measured is only valid for vessels with a diameter less than 300 μm. This depth may be reduced as the angle between the flow direction and the sample arm beam is increased [20]. This would have to be taken into account when translating these results to *in vivo* studies in the human microcirculation.

6. Summary

The results from this investigation show that DOCT can indeed be used to detect the presence of blood flow over a physiologically relevant depth range within a medium with optical properties similar to those found in the tissues surrounding the human cutaneous microcirculation. Although the presence of flow can be detected at depths up to 1 mm within the scattering media, it is less plausible that measurements of the subtle flow dynamics within a capillary of diameter similar to that investigated in this study could be carried out *in vivo* at depths greater than 150 μm.

References

[1] Izatt J A and Kulkarni M D 1996 Doppler flow imaging using optical coherence tomography *Conf. on Lasers and Electro-Optics* (*OSA Technical Digest Series* vol 9) (Washington, DC: Optical Society of America)

[2] Izatt J A, Sivak M V, Kulkarni M D, Yazdanfar S and Rollins A M 1999 Doppler flow imaging using optical coherence tomography *US Patent Specification* 006128

[3] Chen Z, Milner T E, Srinivas S, Wang X, Malekafzali A, van Gemert M J C and Nelson J S 1997 Noninvasive imaging of *in vivo* blood flow velocity using optical Doppler tomography *Opt. Lett.* **22** 1119–21

[4] Wang X, Milner T E, Chen Z and Nelson J S 1997 Measurement of fluid-flow-velocity profile in turbid media by the use of optical Doppler tomography *Appl. Opt.* **36** 144–9

[5] Wang X, Milner T E and Nelson J S 1995 Characterisation of fluid flow velocity by optical Doppler tomography *Opt. Lett.* **20** 1337–9

[6] Chen Z, Milner T E, Dave D and Nelson J S 1997 Optical Doppler tomographic imaging of fluid flow velocity in highly scattering media *Opt. Lett.* **22** 64–6

[7] Yang V X D, Gordon M, Qi B, Pekar J, Lo S, Seng-Yue E, Mok A, Wilson B and Alex Vitkin I 2003 High speed, wide velocity dynamic range Doppler optical coherence tomography (Part I): system design, signal processing, and performance *Opt. Express* **11** 794–809

[8] van Leeuwen T G, Kulkarni M D, Yazdanfar S, Rollins A M and Izatt J A 1999 High-flow velocity and shear-rate imaging by use of color Doppler optical coherence tomography *Opt. Lett.* **24** 1584–6

[9] Chen Z, Milner T E, Wang X, Srinivas S and Nelson J S 1998 Optical Doppler tomography: imaging *in vivo* blood flow dynamics following pharmacological intervention and photodynamic therapy *Photochem. Photobiol.* **67** 56–60

[10] Leigeb R A, Schmetterer L, Drexler W and Fercher A 2003 Real-time assessment of retinal blood flow with ultrafast acquisition by color Doppler Fourier domain optical coherence tomography *Opt. Express* **11** 3116–21

[11] Moger J, Matcher S J, Winlove C P and Shore A 2004 Measuring red blood cell flow dynamics in a glass capillary using Doppler OCT and Doppler amplitude OCT *J. Biomed. Opt.* **9** 982–94

[12] Baker M and Wayland H 1974 On-line volume flow rate and velocity profile measurement for blood in microvessels *Microsvac. Res.* **7** 131–43

[13] Tangelder G J, Slaff D W, Muijtjens A M M, Arts T J, oude Egbrink M G A and Reneman R S 1986 Velocity profiles of blood platelets and red blood cells flowing in arterioles of the rabbit mesentery *Circulation Res.* **59** 505–14

[14] Slaff D W, Arts T, Jeurens T J M, Tangelder G J and Reneman R S 1984 Electronic measurement of red blood cell velocity and volume flow in microvessels *Investigative Microtechniques in Medicine and Biology* ed J Chayen and L Bitensky (New York: Dekker) pp 327–64

[15] Tearney G J, Bouma B E and Fujimoto J G 1997 High speed phase- and group-delay scanning with a grating based phase control delay line *Opt. Lett.* **22** 1811–13

[16] van Staveren H, Moes C, van Marle J and Prahl S 1991 Light scattering in intraplid-10% in the wavelength range of 400–1100 nm *Appl. Opt.* **30** 4507–14

[17] Cheong W, Prahl S A and Welch A J 1990 A review of the optical properties of biological tissues *IEEE J. Quantum Electron.* **26** 2166–85

[18] Meglinsky I V and Matcher S J 2000 Computational model of human skin for reflected spectra simulation *Satatov Fall Meeting '99: Optical Technology and Medicine*, *Proc. SPIE* **4001**

[19] Caro C G, Pedley T J, Schroter R C and Seed W A 1978 *The Mechanics of the Microcirculation* (Oxford: Oxford University Press)

[20] Lindmo T, Smithies D J, Chen Z, Nelson J S and Milner T E 1998 Accuracy and noise in optical Doppler tomography studied by Monte Carlo simulation *Phys. Med. Biol.* **43** 3045–64